ACS APPLIED MATERIALS & INTERFACES

RESEARCH ARTICLE

www.acsami.org

Induction of Apoptosis in Cancer Cells at Low Silver Nanoparticle Concentrations using Chitosan Nanocarrier

Pallab Sanpui,[†] Arun Chattopadhyay,[*,†,§] and Siddhartha Sankar Ghosh[*,†,‡]

[†]Centre for Nanotechnology, [‡]Department of Biotechnology, and [§]Department of Chemistry, Indian Institute of Technology Guwahati, Guwahati-39, Assam, India

Supporting Information

ABSTRACT: We report the development of a chitosan nanocarrier (NC)-based delivery of silver nanoparticles (Ag NPs) to mammalian cells for induction of apoptosis at very low concentrations of the NPs. The cytotoxic efficacy of the Ag NP-nanocarrier (Ag-CS NC) system in human colon cancer cells (HT 29) was examined by morphological analyses and biochemical assays. Cell viability assay demonstrated that the concentration of Ag NPs required to reduce the viability of HT 29 cells by 50% was 0.33 μg mL^{-1}, much less than in previously reported data. The efficient induction of apoptosis by Ag-CS NCs was confirmed by flow cytometry. Additionally, the characteristic nuclear and morphological changes during apoptotic cell death were investigated by fluorescence and scanning electron microscopy (SEM), respectively. The involvement of mitochondrial pathway of cell death in the Ag-CS NCs induced apoptosis was evident from the depolarization of mitochondrial membrane potential ($\Delta\Psi_m$). Real time quantitative RT-PCR analysis demonstrated the up-regulation of caspase 3 expression which was further reflected in the formation of oligo-nucleosomal DNA "ladders" in Ag-CS NCs treated cells, indicating the important role of caspases in the present apoptotic process. The increased production of intracellular ROS due to Ag-CS NCs treatment indicated that the oxidative stress could augment the induction of apoptosis in HT 29 cells in addition to classical caspase signaling pathway. The use of significantly low concentration of Ag NPs impregnated in chitosan nanocarrier is a much superior approach in comparison to the use of free Ag NPs in cancer therapy.

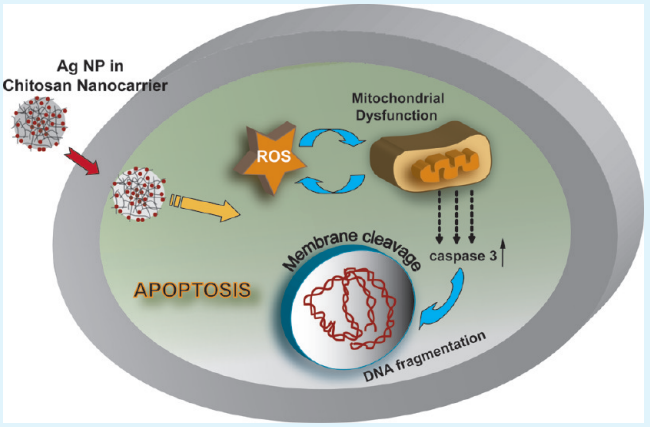

KEYWORDS: silver nanoparticle, chitosan nanocarrier, apoptosis, mitochondrial membrane potential, reactive oxygen species

INTRODUCTION

Successful applications of metal and semiconductor nanoparticles (NPs) in therapeutics,[1−5] biodiagnostics,[6] bioimaging,[7−9] and creation of functional nanodevices[10] demand clear understanding of the fundamental processes involved in the interactions between nanoscale materials and mammalian or bacterial cells. Furthermore, the development of a suitable vehicle for efficient delivery of nanomaterials constitutes an important goal in this regard. For example, silver nanoparticles (Ag NPs) have been proposed for use as potential antimicrobial and anticancer agents, especially in emergency situations. In this regard, the first Food and Drug Administration (FDA) approved Ag NP-based bandage for treating burn wounds, under the trade name Acticoat, is already in commercial use.[11] On the other hand, substantial research from the laboratories of ours[12−14] and others[15−20] has successfully demonstrated the superior antimicrobial efficacy of Ag NPs either as is or in composites with polymer. Additionally, the possibility of using Ag NPs, by themselves or in combination with gene therapy, to induce apoptosis in mammalian cells has been explored recently by our group.[21,22] The fundamental understanding gained in these studies indicated that the Ag NPs, apart from disrupting normal cellular function and affecting the membrane integrity, induced various apoptotic signaling genes of mammalian cells leading to programmed cell death. Hsin et al.[23] have recently reported that Ag NPs induced apoptosis in NIH3T3 cells by heightening the ROS generation and activated JNK pathway leading to mitochondria dependent apoptosis. This therapeutically promising aspect of Ag NPs to induce apoptosis can effectively be exploited in the field of nanomedicine as the genetically programmed cell death or apoptosis, which eliminates the unwanted or damaged cells in the process of development or in response to infection or DNA damage,[24] is critical to develop viable therapeutics for fighting against killer diseases such as cancer and autoimmune diseases.[25]

Received: September 6, 2010
Accepted: January 2, 2011
Published: January 31, 2011

The DNA damaging ability and possible genotoxicity of Ag NPs reported in recent studies[26,27] pose critical issues in the therapeutic implications of Ag NPs. The oxidative stress which has been demonstrated to be responsible for the DNA damage in these studies is also a major contributing factor toward apoptotic cell death.[28] Conventional anticancer therapies suffer from lack of generality, ineffectiveness in case of advanced stages of the disease, and numerous toxic side effects left by radiation or chemicals used in the process.[29,30] The level of toxicity associated with the use of Ag NPs, hence, may not necessarily be graver than those mentioned above and thus could be considered for alternative therapy. An ideal scenario would be the one where a carrier could be developed not only for efficient delivery but also for high efficacy of Ag NPs at their lowest possible concentrations. In this regard, nanocarriers (NCs) have recently emerged as potential drug-carriers in cancer therapy due to increased drug efficacy, low toxicity, and continued steady-state therapeutic level of drug in drug− nanocarrier systems.[31] Among various NC-systems namely inorganic NPs, dendrimers, liposomes, polymeric NPs or micelles and biomolecules,[32−34] polymeric NCs are of particular interest because of the available functional groups in the polymers providing the platform for possible targeted delivery. In this regard, the potential of chitosan for developing biocompatible NCs of conventional anticancer drugs, DNA, and other therapeutically important molecules has already been well established.[35,36] However, chitosan NCs have not been used as such for metal NP delivery. The development of a chitosan-based NC system for Ag NPs, thus, could lead to increased therapeutic index of Ag NPs as a result of improved bioavailability and thereby overall decrease in toxicity.

Herein, we report on developing a novel chitosan-based nanocarrier of Ag NPs (Ag-CS NC) where Ag NPs are homogeneously confined within the biodegradable nanosphere and demonstrate efficient Ag-CS NC-induced apoptosis in human HT 29 colon cancer cells. The apoptotic cell death was investigated by conventional AO/EB dual staining and electron microscopy. Flow cytometric quantification along with cell viability assay revealed that the apoptosis could be successfully induced in HT 29 cells by Ag NPs (being present in the NC) at a concentration way below the previously reported values. The interplay of the pro-apoptotic caspase 3 and antiapoptotic Bcl 2 in the apoptotic process has been shown by semiquantitative RT-PCR as well as quantitative real time RT-PCR. To appreciate the multiplex origin of apoptosis, the effect of Ag-CS NCs on the cellular oxidative stress and mitochondrial membrane potential (MMP) was also investigated. Essentially, the results indicate that the Ag-CS NCs reported here are efficient in inducing programmed cell death with the minimization of toxicity due to the very low concentrations of Ag NPs.

MATERIALS AND METHODS

Synthesis of Silver Nanoparticle-Chitosan Nanocarrier (Ag-CS NC). Chitosan-stabilized Ag NPs (chitosan-Ag NPs) were synthesized as described previously.[37] Chitosan nanocarriers were prepared according to the process developed by Calvo et al.[38] based on the ionotropic gelation of chitosan (Sigma-Aldrich, viscosity average molecular weight, M_v, 672 kDa and degree of deacetylation >75%) by tripolyphosphates (TPP). Briefly, Ag-CS NCs were synthesized by adding aqueous TPP solution (0.4 mg mL^{-1}) to chitosan-Ag NP composite solution (1.5 mg mL^{-1}) under magnetic stirring at room temperature. The residual Ag^+ ions, if any, present in the Ag-CS NC preparation were completely removed (Supporting Information, Figure S1). Blank chitosan nanocarriers (CS NCs) were also prepared in the same procedure except chitosan solution, instead of chitosan-Ag NP composite, was taken.

The morphology of the CS NCs and Ag-CS NCs was investigated by a LEO1430VO scanning electron microscope (SEM) by depositing 10 μL of nanoparticle sample on a glass slide followed by air drying. The slides were coated with gold film with a Polaron Sputter Coater before analyzing under SEM. For transmission electron microscopy (TEM), 5 μL of different liquid nanoparticle samples were drop cast on carbon-coated copper TEM grids and subsequently air-dried at room temperature. The grids were then analyzed by a JEOL 2100 UHR-TEM instrument operating at an accelerating voltage of 200 KeV. The histograms for particle size distribution were constructed by analyzing several TEM images. The UV−visible spectra of the samples were recorded in a Perkin-Elmer Lambda-45 spectrophotometer at room temperature. The amount of Ag NPs present in the Ag-CS NCs was determined by atomic absorption spectroscopy (AAS) in a Varian AA240 atomic absorption spectrophotometer.

Cell Culture and Ag-CS NCs Treatment. HT 29 cells (human adenocarcinoma) were procured from National Center for Cell Sciences (NCCS), Pune, India and were cultured in Dulbecco's modified Eagle's medium supplemented with L-glutamine (4 mM), penicillin (50 units mL^{-1}), streptomycin (50 mg mL^{-1}), and 10% (v/v) fetal bovine serum. Cells were maintained in 5% CO_2 humidified incubator at 37 °C. The stock solutions of Ag-CS NCs and blank CS NCs (2 mg mL^{-1}) were prepared in sterile phosphate-buffered saline (PBS). Required volumes of Ag-CS NCs and CS NCs stock solution were added to the cultures to obtain appropriate concentrations of nanocarriers and incubated for 24 h. DMEM was used to dilute the nanocarrier stock to required concentrations. After the treatment with Ag-CS NCs and CS NPs, HT 29 cells were observed under a phase contrast microscope (Nikon ECLIPSE, TS100, Tokyo) to identify the morphological changes as compared to the nontreated cells.

Lactate Dehydrogenase (LDH) Assay. The cytotoxicity of Ag-CS NCs and blank CS NCs was determined by measuring the activity of LDH enzyme, released in culture media due to the treatment, using CytoTox 96 Non-Radioactive Cytotoxicity Assay Kit (Roche Applied Science). Aliquots (50.0 μL) of culture media were collected at different time intervals, diluted with 1:1 fresh medium and incubated with 50.0 μL of tetrazolium salt (INT) solution (substrate) for 30 min at room temperature. As LDH converted INT to the red formazon product, the LDH release was measured at 490 nm with a microplate reader (Bio-Rad model 680; Bio-Rad, CA) as per manufacturer's instructions. The cells treated with 0.8% (v/v) Triton X-100 were used as positive control whereas nontreated cells served as negative control. Cytotoxicity of the test materials was calculated as

$$\%\text{cytotoxicity} = (\text{LDH release in treated cells} - \text{LDH release in negative control})/(\text{LDH release in positive control} - \text{LDH release in negative control}) \times 100$$

5-Carboxyfluorescein Diacetate Succinimidyl Ester (cFDA-SE)−Propidium Iodide (PI) Staining. Viability of Ag-CS NC treated cells was microscopically examined by cFDA-SE (Sigma-Aldrich) staining. cFDA-SE is a membrane-permeable nonfluorescent probe which intracellular esterases convert to a fluorescent

derivative that in turn is covalently bound to intracellular proteins through the probe's succinimidyl group.[39] The stock solution of cFDA-SE (100 μM) was prepared by dissolving in 20 μL of dimethyl sulfoxide (Sigma-Aldrich) and then further diluted in 1 mL of ethanol (Merck India Ltd.). The stock was filter sterilized and stored at −20 °C. Following the nanocarrier treatment, 5 μM cFDA-SE and 10 μg mL^{-1} PI added to the culture plate and incubated for 30 min. The cells were then washed with PBS and fresh DMEM was added to the plates before observation under the fluorescence microscope (Nikon ECLIPSE, TS100, Tokyo).

Viability Assay. Cell viability was quantified by measuring mitochondrial activity by CellTiter 96 Aqueous One Solution Assay kit (Promega, Madison, WI). Respiring mitochondria in viable cells convert tetrazolium compound, MTS [3-(4,5-dimethylthiazol-2yl)-5-(3carboxymethoxyphenyl)-2-(4-sulfophenyl)-2H-tetrazolium] to formazan product in the presence of an electron coupling reagent, phenazine ethosulfate (PES). The quantity of formazan product as measured by the absorbance at 490 nm is directly proportional to the number of living cells in culture. For viability assay, HT 29 cells were seeded in 96-well microtiter plates followed by overnight incubation. After overnight incubation, the cells were treated with different concentrations of the Ag-CS NCs for another 12 h. Twenty μL of Aqueous One solution was then directly added to individual well and further incubated for 2 h. The amount of formazan product was measured by recording A_{490} with a microplate reader (Bio-Rad model 680; Bio-Rad, CA). The cell viability was calculated as

$$\%\text{cell viability} = (A_{490} \text{ in treated sample}/A_{490} \text{ in control sample}) \times 100$$

Transmission Electron Microscopy (TEM). Cells (2×10^6 cells/dish) were seeded in 35-mm tissue culture dishes and grown overnight. After overnight growth, the medium was removed from the plates and fresh medium containing 24 μg mL^{-1} Ag-CS NCs was added. In control sample, medium without Ag-CS NCs was used. After 3 h of incubation, the cells were washed with PBS, trypsinized, and pelleted down by centrifugation. The cell pellet was then washed with PBS followed by fixation in glutaraldehyde/paraformaldehyde solution. The fixed cells were dehydrated in graded ethanol solutions. Finally the cells were resuspended in absolute ethanol and 5 μL of cell suspension was drop-cast on TEM grid followed by air drying. The grids were then analyzed by a JEOL 2100 UHR-TEM instrument.

Acridine Orange/Ethidium Bromide (AO/EB) Staining. The cells treated with Ag-CS NCs were stained with AO/EB (Sigma-Aldrich) dual dye in order to detect apoptotic or necrotic nuclei. Cells were grown in 6-well tissue culture plates for 24 h followed by the Ag-CS NC treatment at desired concentrations. The culture media were then removed and the cells were washed twice with PBS. Fresh media were added in each well and the cells were stained by adding 10 μL of AO/EB mix (10 mg mL^{-1} AO and 10 mg mL^{-1} EB in PBS). After 10 min of incubation, cells were washed with PBS before visualizing under a fluorescence microscope (Nikon ECLIPSE, TS100, Tokyo) with an excitation filter of 480/30 nm.

Scanning Electron Microscopy (SEM). Cells (seeded at a cell density of 1×10^5 cells/mL) were grown in 6-well tissue culture plates and treated with respective concentrations of Ag-CS NCs for 6 h. The cells were then washed with PBS followed by fixation in glutaraldehyde/paraformaldehyde solution. The fixed cells were dehydrated in graded ethanol solutions and air-dried. Finally, a heated metal cutter was used to cut discs from the bottom of the wells on which the cells had been grown. The cells attached on discs were coated with gold film in a Polaron sputter coater and examined in LEO 1430VP SEM.

Annexin V−PI staining. The induction of apoptosis in HT 29 cells by Ag-CS NCs was examined by FITC-labeled annexin V (FITC-annexin V) staining of the treated cells. The cells were simultaneously stained with PI in order to differentiate the necrotic cells from the apoptotic ones based on the membrane integrity. Following the Ag-CS NC treatment, cells were harvested and washed with PBS. The cells were then stained with FITC-annexin V−PI as per manufacturer's instructions (FITC Annexin V Apoptosis Detection Kit, BD Pharmingen, NJ) and analyzed in a FACS Calibur (BD Biosciences, NJ) flow cytometer. The data were collected with Cell Quest Pro software for 15 000 cells in each sample and subsequently analyzed with WinMDI software. A parallel set of FITC-annexin V−PI stained cells was also visualized for apoptosis under a fluorescence microscope (Nikon ECLIPSE, TS100, Tokyo).

Analysis of DNA Fragmentation. Following the treatment with required concentrations of Ag-CS NCs for 12 h, HT 29 cells were collected, washed with PBS, and lysed (Lysis solution: 10 mM Tris-HCl pH 7.4, 10 mM EDTA and 0.5% Triton X-100). Cell lysates were then incubated with RNase A (200 mg mL^{-1}; Bioline, USA) for 1 h, followed by proteinase K (200 mg mL^{-1}; Bioline, USA) treatment for 1 h at 37 °C. After extracting the samples with phenol/chloroform/isoamyl alcohol (25:24:1, v/v/v) followed by chloroform, DNA was precipitated in two volumes of ethanol in the presence of 0.3 M sodium acetate at −20 °C. Finally the DNA samples were run on 1.5% agarose gel at 60 V and visualized by ethidium bromide staining under UV light.

Semiquantitative RT-PCR and Real Time Quantitative RT-PCR Analysis. For gene expression analysis, HT 29 cells (2×10^5 cells/well in a 6-well plate) were grown for 24 h and subsequently treated with required amount of Ag-CS NCs. Expression of apoptotic signaling genes, Bcl 2 and caspase 3, was examined using reverse transcriptase−polymerase chain reaction (RT-PCR). The housekeeping gene β actin was used as internal control. Total RNA was isolated from entire cell population in each well using Tri reagent (Sigma-Aldrich, USA). cDNA was generated from total denatured RNA (3 μg) by reverse transcription performed at 37 °C for 50 min using M-MLV Reverse Transcriptase (Sigma-Aldrich, USA) in a total mixture of 20 μL. Semiquantitative PCR was carried out with 2 μL of the above RT product using the gene-specific upstream and downstream primers in Gene Amp PCR system 9700, Applied Biosystems. Initial denaturation (94 °C for 2 min) was followed by a PCR cycle of denaturation (94 °C for 15 s), annealing (55 °C for 30 s), extension (68 °C for 1 min), and final extension (68 °C for 5 m). The PCR products were finally resolved on a 1.2% agarose gel and visualized by ethidium bromide staining under UV light.

For real time PCR reaction, reactions were performed with 2 μL of cDNA sample in a total volume of 25 μL including SYBR Green PCR master mix (Applied Biosystems, CA) according to manufacturer's instructions. Amplification was carried out in an Applied Biosystems 7500 Real-Time PCR System, keeping cycle parameters the same as above except the initial denaturation was performed at 95 °C for 10 min (for activation of Ampli-Taq Gold present in SYBR Green PCR master mix). Each PCR reaction was performed in triplicate. Relative quantification of the target gene transcripts normalized to endogenous control β actin and

relative to a calibrator (nontreated control cells) was calculated by SDS software (provided with the Applied Biosystems 7500 Real-Time PCR System) based on $\Delta\Delta C_T$ method. Thus the gene expression in control sample has a value of 1 and expression in treated sample is expressed as an *n*-fold difference relative to control. The primers used were β actin forward: 5′-CTGTCTGGCGGCACCACCAT-3′ and reverse: 5′-GCAACTAAGTCATAGTCCGC-3′, Bcl 2 forward: 5′-AGATGTCCAGCCAGCTGCACCTGAC-3′ and reverse: 5′-AGATAGGCACCCAGGGTGATGCAAGCT-3′, and caspase 3 forward: 5′-TTTGTTTGTGTGCTTCTGAGCC-3′ and reverse: 5′-ATTCTGTTGCCACCTTTCGG-3′.

Determination of Mitochondrial Membrane Potential (MMP). HT 29 cells (2×10^5 cells/well in a 6-well plate) grown for 24 h were treated with appropriate concentrations of Ag-CS NCs for 3 h and then incubated with 5 μM of 5,5,6,6-tetrachloro-1,1,3,3-tetraethylbenzimidazolylcarbocyanine iodide (JC-1; Sigma-Aldrich, USA) for 30 min in the CO_2 incubator. After the incubation the cells were washed twice with prewarmed PBS, harvested, and analyzed with a flow cytometer (FACSCalibur; BD Biosciences). The JC 1 fluorescence data were recorded with the CellQuest program (BD Biosciences) for 20 000 cells in each sample and subsequently analyzed by WinMDI software. A parallel batch of treated cells was stained with JC 1 and washed with PBS before visualization under a fluorescence microscope (Nikon ECLIPSE, TS100, Tokyo).

Determination of Reactive Oxygen Species (ROS). The generation of ROS in Ag-CS NCs treated cells was determined by 2,7-dichlorofluoresceindiacetate (DCFH-DA; Sigma-Aldrich, USA) staining. DCFH-DA is nonfluorescent and can diffuse into the cell through the plasma membrane where it is hydrolyzed to DCFH. Nonfluorescent DCFH is finally converted to green fluorescent dichlorofluorescein (DCF) upon intracellular oxidation. For this assay, HT 29 cells were seeded in a 6-well plate (2×10^5 cells/well) and were grown for 24 h. After 24 h of growth, the cells were treated with different concentrations of Ag-CS NCs for 3 h, harvested, and washed twice with PBS. Finally, the cells were resuspended in 1 mL of DMEM with 5 μM DCFH-DA and incubated for 10 min at 37 °C. Stock (1 mM) solution of DCFH-DA was prepared in ethanol and stored under liquid nitrogen vapor. Immediately after the incubation, the samples were analyzed for DCF fluorescence in a flow cytometer (FacsCalibur, BD Biosciences, NJ) at an excitation wavelength of 488 nm and emission wavelengths of 530. The fluorescence data were recorded with the CellQuest program (BD Biosciences) for 20 000 cells in each sample. Flow cytometric data were analyzed using WinMDI software and the ROS generation was expressed in terms of percentage of cells with DCF (green) fluorescence. A parallel batch of treated cells was stained with DCFH-DA visualized under a fluorescence microscope (Nikon ECLIPSE, TS100, Tokyo).

Cell Cycle Analysis. Cell cycle analysis was performed by measuring the DNA content of the treated and the control cells in a flow cytometer. HT 29 cells were grown in 100-mm tissue culture dishes followed by Ag-CS NC treatment for 24 h. After treatment, the cells were harvested by trypsinization, washed with PBS, fixed by slowly adding 2 mL of cold 70% ethanol, and finally stored at 4 °C. The cells were then centrifuged and washed in ice-cold PBS. Finally, the cells were stained with PI in RNase (40 μg mL^{-1} PI and 100 μg mL^{-1} RNase A) and incubated at 37 °C for 30 min in the dark. Immediately after the incubation, the samples were analyzed in a FACSCalibur (BD Biosciences, NJ). PI fluorescence data were recorded with the CellQuest program (BD Biosciences) for 20 000 cells in each sample and subsequently analyzed by WinMDI software.

Scheme 1. Schematic Representation of Preparation of Ag-CS NCs

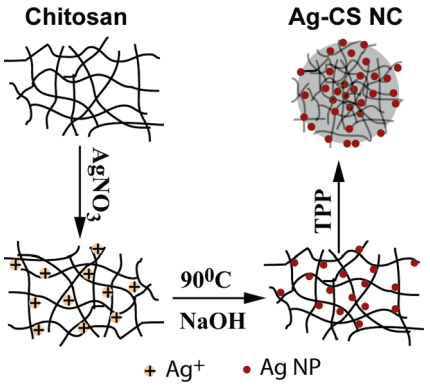

Statistical Analysis. The values for all experiments are expressed as mean ± standard deviation (SD) of three or more individual experiments. The data were analyzed using Student's *t* test, and statistically significant values are denoted by * ($p < 0.05$), ** ($p < 0.005$), and *** ($p < 0.001$).

RESULTS AND DISCUSSION

Characterization of Ag-CS NCs. The Ag-CS NCs used in the present study were prepared via ionic gelation of bulk CS-Ag NP composite by tripolyphosphate (TPP) as shown in Scheme 1. The average size of Ag-CS NCs was estimated to be 172.6 nm (±27.1 nm) from the SEM images (Figure 1a). On the other hand, the blank CS NCs (Figure S2, Supporting Information) synthesized for the control cytotoxicity experiments were 136.9 nm (±28.5 nm) in size. The size of the NC system plays an important role in the delivery of anticancer drugs, as the NPs up to ~400 nm can easily extravasate through the defective vasculature system in the tumor tissues and subsequently accumulate in the tumor microenvironment in presence of ineffective lymphatic clearance.[31] This process is known as "enhanced permeability and retention (EPR)" effect and forms the basis of "passive targeting" for in vivo delivery of anticancer drugs encapsulated in polymeric nanocarriers. The Ag-CS NCs prepared in the present study, hence, meet the size limit to be exploited as a drug delivery system. Recently, Lee et al.[40] have demonstrated successful delivery of siRNA to HEK 293FT and HeLa cells using chitosan/polyguluronate nanocarriers of size ranging from 110 to 430 nm.

The UV−visible absorption spectrum of Ag-CS NCs (Figure 1b) exhibited a strong absorption band at ca. 409 nm corresponding to characteristic surface plasmon resonance (SPR) of metallic Ag NPs.[6] The sharp SPR band of Ag NPs indicated the presence of well separated Ag NPs with narrow size distribution in Ag-CS NCs. This was further confirmed by the TEM image of Ag-CS NCs (Figure 1b, inset) which revealed that the Ag NPs were homogenously incorporated into the chitosan nanocarriers and mostly spherical in shape having a mean size of 4.9 nm (±1.6 nm) with narrow size-dispersion (Figure S3, Supporting Information). The selected area electron diffraction (SAED) pattern (Figure 1b inset) indicated the polycrystallinity of these Ag NPs. The powder XRD pattern of Ag-CS NCs (Figure S4, Supporting Information) also demonstrated the presence of nanosized crystalline Ag NPs in Ag-CS NCs. The

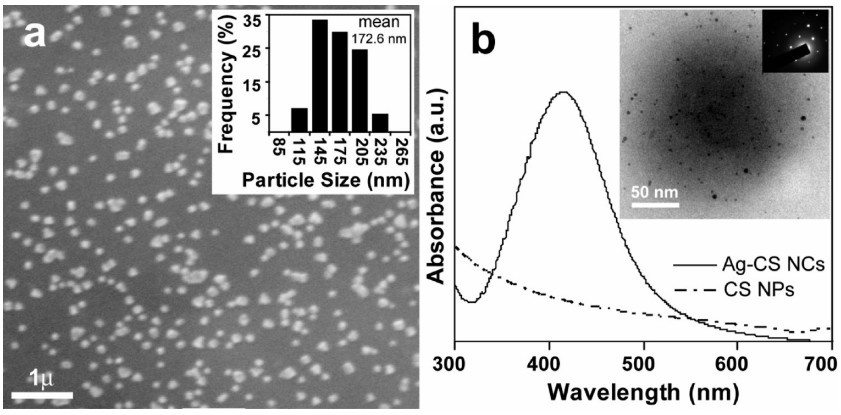

Figure 1. (a) Typical SEM image of Ag-CS NCs. (Inset) Particle size distribution calculated based on the SEM images and mean particle size was found to be 172.6 nm. (b) UV−visible absorption spectra of Ag-CS NCs and blank chitosan nanocarriers (CS NPs). (Inset) Typical TEM image of an Ag-CS NC with corresponding SAED pattern.

loading of the Ag NPs in Ag-CS NCs, as determined by atomic absorption spectroscopy (AAS), was found to be 1.5% (w/w). It may be mentioned here that the stability of Ag-CS NCs in cell culture medium was confirmed (Figure S5, Supporting Information) before carrying out cell-based experiments. This was further supported by a very low level of Ag NP release from the Ag-CS NCs in PBS as shown in Figure S5c.

Cytotoxicity. To examine the cytotoxic effect of Ag CS NCs, the morphology of treated HT 29 cells was observed under phase contrast microscope and distinct morphological changes were detected in treated cells (Figure S6). More cells appeared to be rounded, shrunken, and loosely attached to the surface as the concentration of the Ag-CS NCs increased to 40 μg mL^{-1}. The intercellular connections also decreased notably. At a concentration of 80 μg mL^{-1} or above, treated cells were mostly swollen and detached from neighbor cells with completely disintegrated membrane indicating extensive necrotic cell death at these concentrations. However, HT 29 cells treated with blank CS NCs (80 μg mL^{-1}) showed healthy and normal morphology as compared to the control cells.

The cytotoxicity of Ag-CS NCs on HT 29 cells was measured quantitatively by LDH assay. The results (Figure 2) demonstrate the concentration- and time-dependent leakage of LDH from HT 29 cells exposed to Ag CS NCs. Moreover, the insignificant LDH release in cells treated with blank CS NPs for 12 h confirmed the cyto-compatibility of the chitosan nanocarriers (Figure 2, inset) in the present experimental concentration range.

Cell Viability. The effect of Ag-CS NCs on the viability of HT 29 cells was assessed microscopically by cFDA-SE/PI staining of the treated cells. The result of cFDA-SE/PI staining (Figure S7) clearly shows that the number of viable cells decreased with increasing concentration of Ag CS NCs, as evident from the gradual increase in number of PI-stained (red) cells. Additionally, MTS assay was carried out in order to determine the cell viability quantitatively in Ag CS NCs treated cells and the results are shown in Figure 3. The results show the inhibition of cell viability by Ag CS NCs in a concentration-dependent manner. The IC_{50} value of Ag CS NCs was calculated to be 22 μg mL^{-1}. Based on the IC_{50} value, three different concentrations of Ag-CS NCs namely 12 μg mL^{-1} (~1/2 IC_{50}), 24 μg mL^{-1} (~IC_{50}), and 48 μg mL^{-1} (~2 IC_{50}) were chosen for further apoptosis experiments. Also, a 6 h "NC-treatment" was chosen based on LDH and MTS assay, to study the apoptotic cell death when

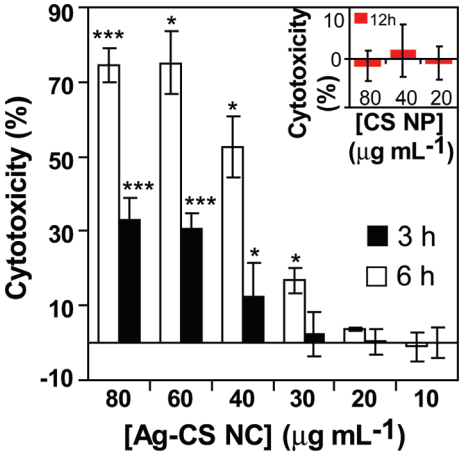

Figure 2. Cytotoxicity of different concentrations of Ag-CS NCs on HT 29 cells after 3 and 6 h of treatment, as calculated from the LDH assay. Cytotoxicity due to blank chitosan nanoparticles after 12 h of treatment is shown in the inset. The values are represented as mean ± SD of three individual experiments. Statistical significance between nontreated control and treated samples is denoted by * ($p < 0.05$) and *** ($p < 0.001$).

most of the cells would manifest the "apoptotic cues" while still maintaining their structural integrity. However, a shorter time duration of 3 h was set for investigating the changes in the MMP and ROS to elucidate the onset of the apoptosis process. It may be mentioned here that the concentration of Ag NPs in Ag-CS NCs at IC_{50} value, as determined by AAS, was found to be 330 ng mL^{-1}. The concentration of Ag NPs required to reduce cell viability by 50% in the present study is less than previously reported values[18,21,23,26,41,42] by orders of magnitude (Table S1, Supporting Information). This extraordinarily high degree of cell death caused by low concentration of Ag NPs in the present study could be due to the increased bioavailability of the Ag NPs impregnated in chitosan NCs which, unlike free Ag NPs, prevent Ag NPs from premature interaction with biological environment as well as help in intracellular uptake.[31]

Uptake of Ag-CS NCs. The uptake of Ag-CS NCs by HT 29 cells was investigated by TEM analysis of treated cells. The TEM image of nontreated control cells (Figure S9, Supporting Information) showed healthy cellular morphology. On the other hand, TEM image of HT 29 cells treated with 24 μg mL^{-1}

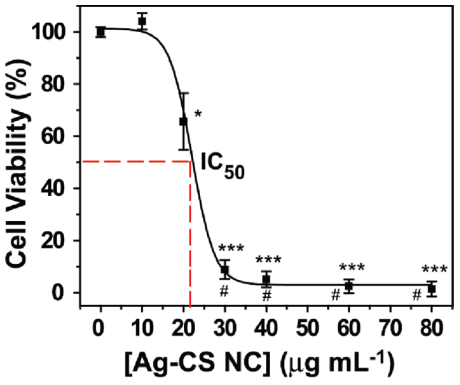

Figure 3. Cell viability of HT 29 cells after 12-h treatment with different concentrations of Ag-CS NCs, as calculated from the MTS assay. The values are represented as mean ± SD of three individual experiments. Statistical significance between nontreated control and treated samples is denoted by * ($p < 0.05$) and *** ($p < 0.001$); statistical significance compared to blank CS NPs (80 μg mL^{-1}) treated sample is denoted by # ($p < 0.05$).

(~IC_{50}) Ag-CS NCs shown in Figure 4a indicated that the Ag-CS NCs were internalized by HT 29 cells. A better view of the image, at higher magnification (Figure 4b), clearly demonstrates the successful delivery of Ag NPs inside the cells by the chitosan nanocarriers. The average dimension of the particles matched that of as-synthesized NPs (Figure 1b) confirming not only the intake of the particles but also retention of their shapes and sizes without further agglomeration in the process. However, further experiments are needed to elucidate the uptake mechanism completely, which is outside the scope of the present work. Based on the TEM images, it was estimated that Ag-CS NCs delivered about 1.6×10^3 Ag NPs ($\sim 1.1 \times 10^{-5}$ ng Ag NPs) to a single HT 29 cell at ~IC_{50} concentration. This was pursued by counting the number of Ag NPs actually present in the cells (averaged over 15 cells) as viewed under TEM.

Mode of Cell Death. To investigate the mode of cell death (viz. apoptosis or necrosis) in HT 29 cells caused by the Ag-CS NCs, treated cells were stained with AO/EB dual dye and observed under the fluorescence microscope. Figure 5b shows that the cells treated with 12 μg mL^{-1} Ag-CS NCs, like the nontreated ones (Figure 5a), are uniformly green with normal morphology. However, extensive nuclear margination accompanied with chromatin condensation and fragmentation, distinctive of apoptotic cell death[43,44] was observed in treated cells at the Ag-CS NCs concentrations of 24 and 48 μg mL^{-1}. The images in Figure 5c and 5d clearly demonstrate the presence of early apoptotic cells having condensed chromatin as well as late apoptotic cells with fragmented chromatin and apoptotic bodies. The results of AO/EB nuclear staining indicated the induction of apoptosis in HT 29 cells by Ag-CS NCs.

Complementary to the AO/EB staining, Ag-CS NC treated HT 29 cells were further examined under the SEM in the quest of the characteristic morphological changes observed during apoptosis. Figure 6a shows the typical morphology of healthy HT 29 cells that are well-attached to the surface. The cells treated with 12 μg mL^{-1} (~1/2 IC_{50}) Ag-CS NC showed healthy morphology (Figure 6b) whereas the cells treated with 24 μg mL^{-1} (~IC_{50}) and 48 μg mL^{-1} (~2 IC_{50}) of Ag-CS NC demonstrated round-shaped and loosely attached cells (Figure 6c and 6d) as compared to nontreated cells. The occurrence of membrane blebbing as well as formation of apoptotic bodies, indicative of

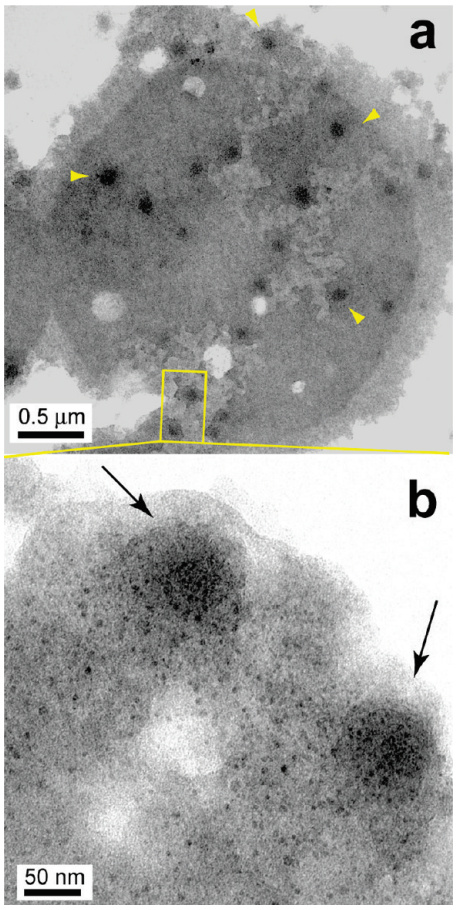

Figure 4. (a) TEM image of HT 29 cells treated with Ag-CS NCs (24 μg mL^{-1}) showing successful internalization of Ag-CS NCs (indicated by yellow arrow-heads) by the cells. (b) Magnified view of the selected region inside the cell demonstrating the release of Ag NPs by two chitosan nanocarriers (indicated by black arrows). Ag NPs can be seen as the black contrasted small dots.

apoptotic cell death,[43,44] was clearly detected in HT 92 cells treated with Ag-CS NCs (at IC_{50} and 2 IC_{50}).

Annexin V−PI staining. The apoptotic cell death in HT 29 cells induced by Ag-CS NCs was confirmed and subsequently quantified by microscopic and flow cytometric analysis of annexin V−PI stained HT 29 cells, respectively. Early apoptotic cells can easily be identified by green fluorescence of FITC-conjugated annexin V as annexin V has a high affinity toward phosphatidyl serine (PS) residues which are externalized from inner to outer leaflet of the plasma membrane during early stages of apoptosis.[45,46] Due to its membrane impermeability, PI, on the other hand, helps in identifying the necrotic and late apoptotic cells having damaged plasma membrane.[44,46] The fluorescence microscopic images of FITC-annexin V−PI stained HT 29 cells (Figure 7a−h) revealed that the cells treated with 12 μg mL^{-1} Ag-CS NCs were almost unaffected as compared to nontreated control cells. However, the induction of apoptosis in HT 29 cells by Ag-CS NCs at the concentrations of 24 and 48 μg mL^{-1} is evident from the presence of green fluorescent early apoptotic cells and red−green dual fluorescent late apoptotic cells in Figure 7c and d. Figure 7i shows the results of flow cytometric analysis of FITC-annexin V−PI stained HT 29 cells treated with different concentrations of Ag-CS NCs. The percentages of apoptotic and necrotic population in treated and untreated cells

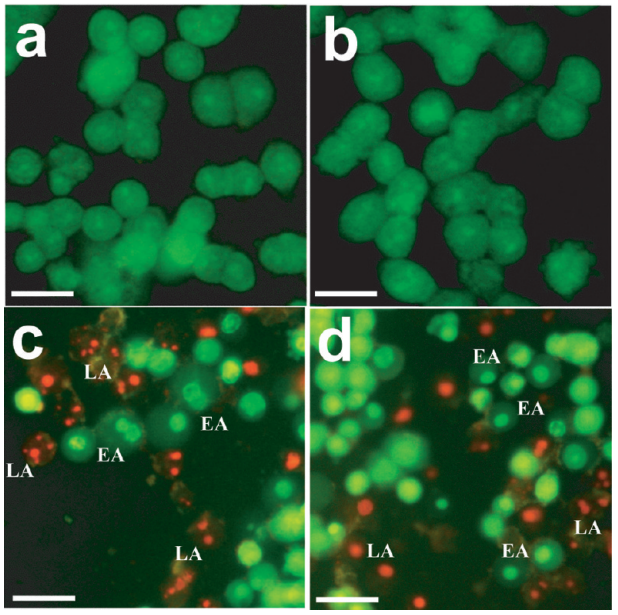

Figure 5. Representative images of AO/EB dual staining of (a) nontreated, (b) 12 μg mL^{-1} (~1/2 IC_{50}), (c) 24 μg mL^{-1} (~ IC_{50}), and (d) 48 μg mL^{-1} (~2 IC_{50}) Ag-CS NCs treated HT 29 cells after 6 h of treatment. Condensed chromatin in early apoptotic (EA) cells and fragmented chromatin in late apoptotic (LA) cells are clearly visible in (c) and (d). Scale bar: 20 μm.

were calculated from the flow cytometric data and are summarized in Figure 7j. Figure 7j clearly shows the dose-dependent reduction in cell viability of HT 29 cells in presence Ag-CS NCs. Most importantly, the apoptotic population in HT 29 cells increased by ca. 34% and ca. 61% in presence of 24 and 48 μg mL^{-1} Ag-CS NCs, respectively. On the other hand, an increase of ca. 8% and ca. 2.5%, respectively, was observed in necrotic population at these concentrations. The results of flow cytometric analysis clearly establish the efficient induction of apoptotic cell death in HT 29 cells by Ag-CS NCs.

DNA Fragmentation and Up-Regulation of Caspase 3. The formation of oligo-nucleosomal DNA fragments or "ladder" due to the fragmentation of DNA is widely regarded as a biochemical hallmark of late apoptosis.[44] The DNA fragmentation in the present study was verified by extracting DNA from HT 29 cells treated with Ag-CS NCs followed by detection in the agarose gel. Figure 8a clearly demonstrates the DNA "laddering" pattern in HT 29 cells treated with 24 μg mL^{-1} (~IC_{50}) and 48 μg mL^{-1} (~2 IC_{50}) Ag-CS NCs. On the other hand, cells treated with 12 μg mL^{-1} (~1/2 IC_{50}) Ag-CS NCs did not produce detectable DNA ladder. These results are consistent with flow cytometric data of apoptosis in Ag-CS NC treated HT 29 cells.

Caspases are cysteine-aspartic acid proteases and well-known for their vital role in the initiation as well as the execution of apoptosis.[47] Especially the activation of caspase 3 is crucial for cellular DNA fragmentation.[48] The role of caspase 3 in Ag-CS NC-mediated apoptosis in HT 29 cells was investigated by conventional RT-PCR analysis. The results of semiquantitative RT-PCR (Figure 8b) indicate up-regulation of caspase 3, as compared to house-keeping β actin gene, in HT 29 cells treated with 24 μg mL^{-1} (~IC_{50}) Ag-CS NCs. Additionally, quantitative real-time RT-PCR analysis (Figure 8c) clearly demonstrates that the expression level of caspase 3, normalized to β actin gene as internal

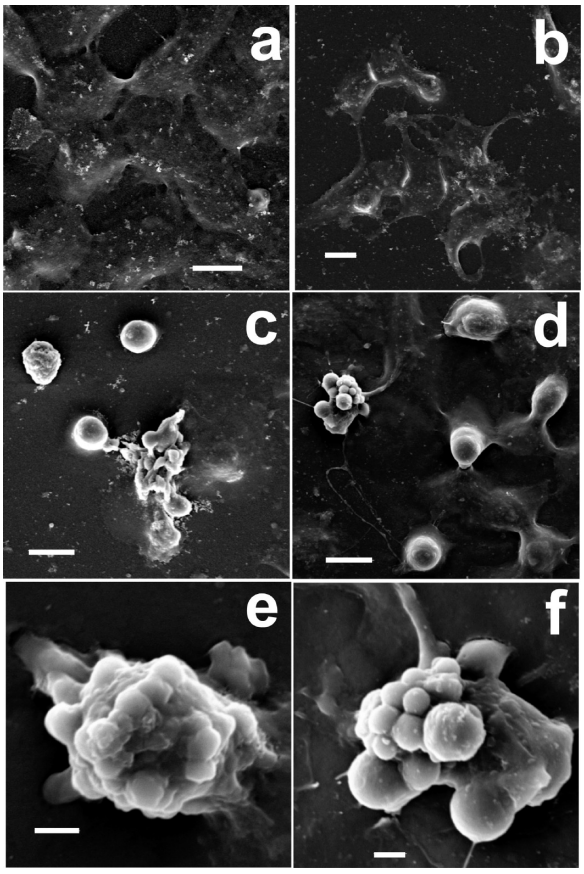

Figure 6. Representative SEM images of (a) nontreated HT 29 cells and cells treated with (b) 12 μg mL^{-1} (~1/2 IC_{50}), (c) 24 μg mL^{-1} (~ IC_{50}), and (d) 48 μg mL^{-1} (~2 IC_{50}) of Ag-CS NCs for 6 h. Images (c) and (d) are shown at higher magnification in (e) and (f), respectively. Morphological changes associated with apoptosis viz. membrane blebbing and formation of apoptotic body are clearly detectable in (c)−(f). Scale bar: 10 μm (a−d) and 2 μm (e, f).

control, increased after exposure to Ag-CS NCs. The results indicate the involvement of the caspase signaling pathway in the apoptotic cell death of HT 29 cells treated with Ag-CS NCs. The elevated caspase 3 activity in Ag NP treated mammalian cells has been also reported by others.[21−23,41] On the other hand, the changes in antiapoptotic Bcl 2 expression in treated HT 29 cells were insignificant, as evident from RT-PCR and real-time quantitative RT-PCR analysis (Figure 8b and c). The importance of up-regulation of Bcl 2 in shielding the apoptotic responses of nanosilver in HCT 116 cells has been recently reported by Hsin et al.[23] The RT-PCR results indicate that the absence of active up-regulation, although not down-regulated, of antiapoptotic Bcl 2 plays a critical role in Ag-CS NC induced apoptosis in HT 29 cells.

Effect on Mitochondrial Membrane Potential (MMP). Mitochondria play a key role in the apoptotic pathway of cell death, and the changes in mitochondrial membrane permeability comprise the early events during apoptosis.[49] As the mitochondrial inner membrane potential decreases during apoptosis, the effect of Ag-CS NC exposure on the mitochondrial membrane potential ($\Delta\psi_m$) of HT 29 cells in the present study was further investigated by JC 1 staining. JC 1 is a cationic lipophilic dye that stains polarized mitochondria in viable cells as red due to the formation of J-aggregates emitting red fluorescence.[50] On the

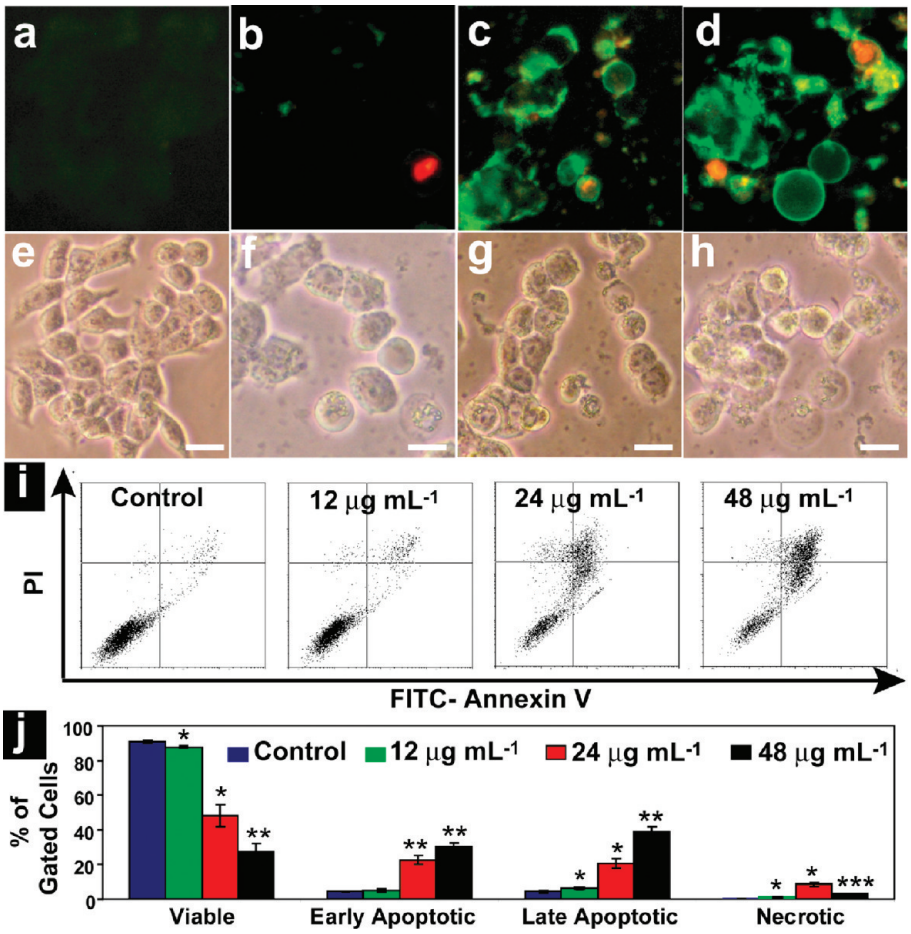

Figure 7. Representative images of FITC-annexin V−PI staining of (a, e) nontreated, (b, f) 12 μg mL^{-1} (~1/2 IC_{50}), (c, g) 24 μg mL^{-1} (~ IC_{50}), and (d, h) 48 μg mL^{-1} (~2 IC_{50}) Ag-CS NCs treated HT 29 cells after 6 h of treatment. The images in the lower panel (e−h) are corresponding bright field images. Scale bar: 10 μm. (i) Flow cytometric analysis of FITC-annexin V−PI stained HT 29 cells after Ag-CS NC treatment. (j) Apoptotic and necrotic populations (%) in each sample were calculated from flow cytometric analysis. The values are represented as mean ± SD of three individual experiments. Statistical significance between nontreated control and treated sample is denoted by * ($p < 0.05$), ** ($p < 0.005$), and *** ($p < 0.001$).

other hand, due to the depolarization of mitochondrial membrane in apoptotic cells, JC 1 remains in its monomeric form and thereby emits green fluorescence. A reduction in the J-aggregate (red fluorescence)/monomer (green fluorescence) ratio, thus, indicates a drop in $\Delta\psi_m$. Fluorescence microscopic observation of control HT 29 cells (Figure 9a) showed completely polarized mitochondria forming J-aggregates as red dots. In contrast, the treatment with Ag-CS NCs resulted in the depolarization of the mitochondrial membrane in HT 29 cells, as evident from the loss of the red dots and simultaneous increase of green fluorescence (Figure 9b−d). Quantitative analysis by flow cytometry (Figure 9i) showed that the MMP in HT 29 cells treated with 24 (IC_{50}) and 48 μg mL^{-1} (2 IC_{50}) of Ag-CS NCs decreased by 43% and 55%, respectively, as compared to that of the control cells. Preferential localization of nanoparticulate fullerenes (C_{60}) in mitochondria has already been reported by Foley et al.[51] As the mitochondrial respiratory chain is the main source of intracellular ROS production in aerobic cells, mitochondrial dysfunction due to NP immobilization may lead to oxidative stress. On the other hand, mitochondrial membrane is among the major susceptible targets of the deleterious effects associated with intracellular ROS. The present results indicate that the adverse changes in mitochondrial function due to Ag-CS NCs, with possible association of intracellular ROS production, trigger the apoptosis process.

Role of ROS. The interaction of engineered nanoparticles with mammalian cells can induce oxidative stress by favoring the cellular ROS production over the cellular antioxidant defenses. Although the exact mechanism is still to be understood, the critical role of ROS in nanoparticle-mediated cytotoxicity and genotoxicity has been recently reported by several researchers.[23,26,42,52−55] To investigate the effect of Ag-CS NC on the cellular ROS production in the present study, the treated cells were examined under microscope for their ability to show green fluorescence of DCF, produced by the intracellular oxidation of DCFH-DA dye. Figure 10 clearly shows the elevation in the ROS production in the Ag-CS NC treated cells compared to the nontreated cells. The increase in ROS generation in treated cells was quantified by determining the percentage of cells with increased green fluorescence in a flow cytometer. It is evident from the flow cytometric analysis (Figure 10i) that Ag-CS NC raised the level of intracellular ROS in a concentration-dependent way and the percentage of cells with elevated ROS increased significantly at 24 and 48 μg mL^{-1} of Ag-CS NC. The present data indicate that Ag-CS NCs, at low concentrations (~ 1/2 IC_{50}), induce modest oxidative stress in HT 29 cells which can be efficiently repaired by intracellular antioxidant response. However, the intracellular ROS level in presence of Ag-CS NC at IC_{50} or more crossed an optimal limit which was toxic enough to

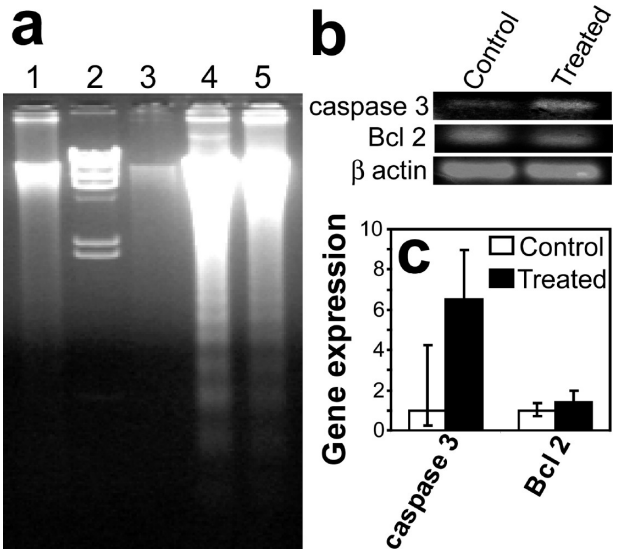

Figure 8. (a) DNA laddering assay of nontreated (lane 3), 12 μg mL^{-1} (lane 1), 24 μg mL^{-1} (lane 4), and 48 μg mL^{-1} (lane 5) Ag-CS NCs treated HT 29 cells. Lane 2: λ DNA/*Hind* III marker. (b) Semiquantitative and (c) real-time quantitative RT-PCR analysis of caspase 3 and Bcl 2 gene in HT 29 cells treated with Ag-CS NCs (24 μg mL^{-1}).

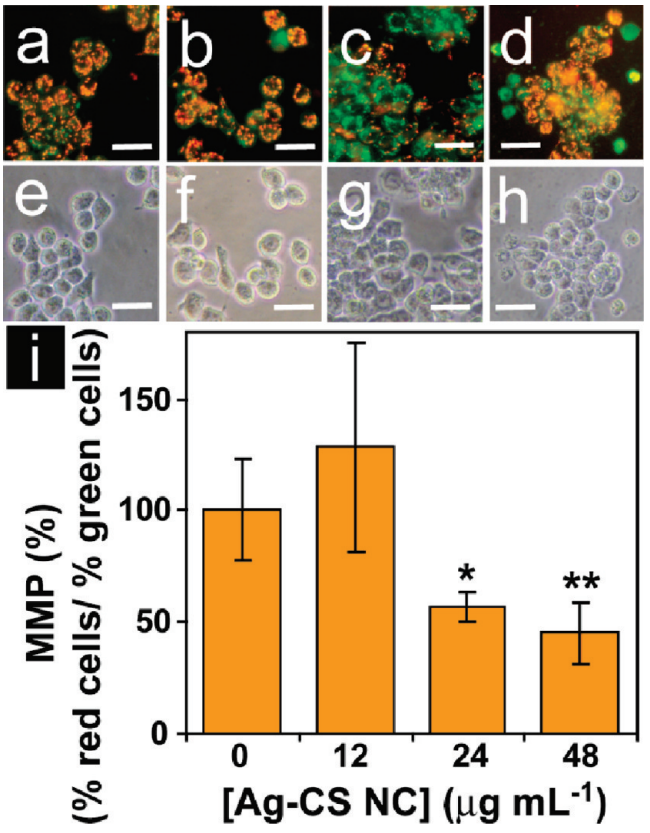

Figure 9. Microscopic image of JC 1 staining of (a, e) nontreated, (b, f) 12 μg mL^{-1} (~1/2 IC$_{50}$), (c, g) 24 μg mL^{-1} (~ IC$_{50}$), and (d, h) 48 μg mL^{-1} (~2 IC$_{50}$) Ag-CS NCs treated HT 29 cells. The images in the lower panel (e−h) are corresponding bright field images. Scale bar: 20 μm. (i) Flow cytometric analysis of MMP in presence of different concentration of Ag-CS NCs. The values are represented as mean ± SD of three individual experiments. Statistical significance between nontreated control and treated sample is denoted by * ($p < 0.05$) and ** ($p < 0.005$).

augment the apoptotic cell death by damaging mitochondrial membrane integrity and increasing oxidative DNA damage.[28] Similar role of ROS in ceramide-induced apoptosis in U937 cells was reported previously by Quillet-Mary et al.[56] where ROS scavengers such as dithiocarbamates (PDTC), *N*-acetylcysteine (thiol antioxidant), and a glutathione (GSH) precursor successfully inhibited the ceramide-induced apoptosis. As the mechanism of ROS generation by nanomaterials remains unclear as mentioned earlier, future studies are required to ascertain the chemical nature of Ag NPs inside the cells in order to determine the contribution of the "nanospecific" physicochemical properties and the chemical toxicity of released silver ions from the Ag NPs in the intracellular ROS production. However, it would be shortsighted at this moment to rule out either of the factors mentioned above, as both have been linked with the cellular toxicity in earlier reports.[41,42,57] Because the Ag NPs remained stable following internalization into the cells (Figure 4) in the present study, it may be that the NPs themselves were primarily responsible for ROS generation rather than Ag^+ ions. However, it cannot be discounted that small amounts of Ag^+, being released from the NCs due to leaching, may also have contributed toward the production of ROS.

In a recent report, Thubagere et al.[58] demonstrated that the polystyrene nanoparticle-induced apoptosis in Caco-2 cells could propagate through H_2O_2-mediated "bystander killing". This finding may promptly lead one to conclude that the Ag NP induced apoptosis in cancer cells could eventually be passed on to the neighboring healthy cells limiting the applicability of the present Ag-CS NC system in cancer therapy, even after achieving tumor targeted delivery of the Ag-CS NCs. However, we must be cautious at this point as the biological effects of nanoscale materials can vary greatly depending upon the physicochemical properties (size, biodegradability, surface-to-volume ratio, surface chemistry, etc.) and the cell type used as the model in vitro system.[59] Furthermore, the "bystander effects", if at all shown by the present Ag-CS NC system, may actually prove to be effective in providing maximum damage to the tumor microenvironment by the tumor-targeted Ag-CS NCs even when the NCs are uptaken by a few cells. To this end, the "bystander killing" has already been demonstrated to eradicate resistant cancer cells[60] and forms the basis of successful "suicide gene therapy" even though the gene transduction efficiency is not optimum.[61]

Effect on Cell Cycle. To investigate the possible DNA damage due to oxidative stress in Ag-CS NC treated HT 92 cells, the cell cycle distribution was monitored by measuring the DNA content in a flow cytometer. Flow cytometric analysis (Figure 11) shows that the cell populations in different phases of cell cycle (G_0/G_1, S, and G_2/M) were mostly unaffected at lower Ag-CS NC concentrations (~1/2 IC and IC$_{50}$), as compared to the nontreated cells. The G_2/M population increased by ca. 3% only when the cells were treated with 48 μg mL^{-1} (~2 IC$_{50}$) Ag-CS NC. However, significant increase in sub-G_0/G_1 population indicates the apoptotic cell death in Ag-CS NC treated cells. Recently, AshaRani et al.[26] reported the profound effect of starch-capped Ag NPs on cell cycle progression, in the form of concentration-dependent G_2/M arrest, in IMR-90 and U 251 cells and related this to the genotoxic effect of the Ag NPs. However, the absence of any significant G_2/M arrest in HT 29 cells in the present study could be due to the fact that the concentrations of Ag NPs (in Ag-CS NCs) tested here are an order of magnitude less. The present results are particularly

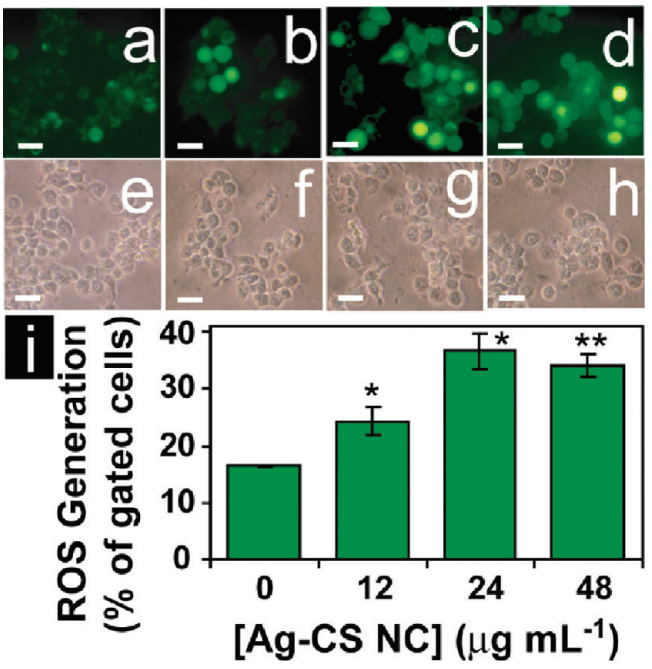

Figure 10. DCFH-DA staining of (a, e) nontreated, (b, f) 12 μg mL^{-1} (~1/2 IC_{50}), (c, g) 24 μg mL^{-1} (~ IC_{50}), and (d, h) 48 μg mL^{-1} (~2 IC_{50}) Ag-CS NCs treated HT 29 cells for visualization of cellular ROS production. The images in the lower panel (e–h) are corresponding bright field images. Scale bar: 20 μm. (i) Flow cytometric analysis of ROS production in presence of different concentration of Ag-CS NCs. The values are represented as mean ± SD of three individual experiments. Statistical significance between nontreated control and treated sample is denoted by * ($p < 0.05$) and ** ($p < 0.005$).

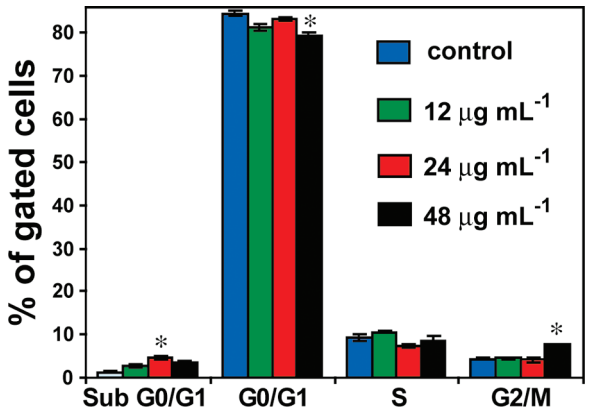

Figure 11. Effect of Ag-CS NCs on cell cycle in HT 29 cells evaluated by calculating the percentage of cells in each phase from flow cytometric data. The values are represented as mean ± SD of three individual experiments. Statistical significance between nontreated control and treated sample is denoted by * ($p < 0.05$).

promising from a therapeutic point of view as the detrimental geno-toxicity of Ag NPs could be avoided without compromising the beneficial apoptosis-inducing efficacy.

CONCLUSION

Ag-CS NCs, as prepared in the present study, were used for the successful delivery of Ag NPs to human HT 29 adenocarcinoma cells. The NCs were found to elicit antiproliferative response at a much lower concentration of Ag NPs (330 ng mL^{-1} at IC_{50}) compared to previously reported data indicating the superior efficacy of the present system. Efficient induction of apoptosis, accompanied by insignificant necrosis, in HT 29 cells by Ag-CS NCs in the concentration range of 24–48 μg mL^{-1} was clearly demonstrated by flow cytometric analysis. The results may prove to be significant in therapeutic applications as the cell death induced by Ag-CS NCs could actually be directed to follow the apoptotic pathway by optimizing the concentration of Ag-CS NCs. The oxidative stress and mitochondrial dysfunction were shown to play an important role in the apoptosis. The cell cycle progression was found to be unaffected by Ag NPs indicating the intimidation of carcinogenesis and genotoxicity being at minimum. The implication of the present findings seems to be promising for the possible application of chitosan-based nanocarriers of Ag NPs to cancer cells, where a synergistic effect of two separate mechanistic pathways—caspase signaling pathway and ROS production—leads to efficient apoptosis. Additionally, this could also help in the wound healing process which is otherwise affected by the inflammatory response elicited by the necrotic cell death. Further studies on the in vivo efficacy of Ag-CS NCs alone or in combination with conventional therapeutic drugs as well as appropriate functionalization of the chitosan NCs in order to achieve target specificity[62] toward cancer cells are currently underway.

ASSOCIATED CONTENT

Supporting Information. Figures S1–S9 and Table S1. This information is available free of charge via the Internet at http://pubs.acs.org.

AUTHOR INFORMATION

Corresponding Author

*E-mail: sghosh@iitg.ernet.in (S.S.G.), arun@iitg.ernet.in (A.C.).

ACKNOWLEDGMENT

This research was supported by the Department of Biotechnology (BT/01/NE/PS/08 and BT/PR9988/NNT/28/76/2007), Department of Science and Technology (SR/S5/NM-01/2005 and 2/2/2005-S.F.) and Council of Scientific and Industrial research (CSIR). P.S. acknowledges CSIR for the fellowship, Abhishek Sahu for helping in SEM, and Amit Jaiswal for helping with the manuscript. Assistance from CIF, IIT Guwahati for SEM and TEM analysis is gratefully acknowledged.

REFERENCES

(1) Norman, R. S.; Stone, J. W.; Gole, A.; Murphy, C. J.; Sabo-Attwood, T. L. *Nano Lett.* **2008**, *8*, 302.

(2) Huang, X.; El-Sayed, I. H.; Qian, W.; El-Sayed, M. A. *J. Am. Chem. Soc.* **2006**, *128*, 2115.

(3) Maltzahn, G.; Park, J.-H.; Agrawal, A.; Bandaru, N. K.; Das, S. K.; Sailor, M. J.; Bhatia, S. N. *Cancer Res.* **2009**, *69*, 3892.

(4) Sun, N. K. C.; Wang, J.; Zhang, M. *Langmuir* **2005**, *21*, 8858.

(5) Jain, T. K.; Morales, M. A.; Sahoo, S. K.; Leslie-Pelecky, D. L.; Labhasetwar, V. *Mol. Pharmaceutics* **2005**, *2*, 194.

(6) Rosi, N. L.; Mirkin, C. A. *Chem. Rev.* **2005**, *105*, 1547.

(7) Lee, J.-H.; Huh, Y.-M.; Jun, Y.; Seo, J.; Jang, J.; Song, H.-T.; Kim, S.; Cho, E.-J.; Yoon, H.-G.; Suh, J.-S.; Cheon, J. *Nat. Med.* **2007**, *13*, 95.

(8) Loo, C.; Lowery, A.; Halas, N.; West, J.; Drezek, R. *Nano Lett.* **2005**, *5*, 709.

(9) Sun, C.; Lee, J. S. H.; Zhang, M. *Adv. Drug Delivery Rev.* **2008**, *60*, 1252.
(10) Fan, H.; Yang, K.; Boye, D. M.; Sigmon, T.; Malloy, K. J.; Xu, H.; López, G. P.; Brinker, C. J. *Science* **2004**, *304*, 567.
(11) Mazurak, V. C.; Burrell, R. E.; Tredget, E. E.; Clandinin, M. T.; Field, C. J. *Burns* **2007**, *33*, 52.
(12) Gogoi, S. K.; Gopinath, P.; Paul, A.; Ramesh, A.; Ghosh, S. S.; Chattopadhyay, A. *Langmuir* **2006**, *22*, 9322.
(13) Sanpui, P.; Murugadoss, A.; Prasad, P. V. D.; Ghosh, S. S.; Chattopadhyay, A. *Int. J. Food Microbiol.* **2008**, *124*, 142.
(14) Banerjee, M.; Mallick, S.; Paul, A.; Chattopadhyay, A.; Ghosh, S. S. *Langmuir* **2010**, *26*, 5901.
(15) Sondi, I.; Salopek-Sondi, B. *J. Colloid Interface Sci.* **2004**, *275*, 177.
(16) Morones, J. R.; Elechiguerra, J. L.; Camacho, A.; Holt, K.; Kouri, J. B.; Ramírez, J. T.; Yacaman, M. J. *Nanotechnology* **2005**, *16*, 2346.
(17) Shrivastava, S.; Bera, T.; Roy, A.; Singh, G.; Ramachandrarao, P.; Dash, D. *Nanotechnology* **2007**, *18*, 225103.
(18) Jain, J.; Arora, S.; Rajwade, J. M.; Omray, P.; Khandelwal, S.; Paknikar, K. M. *Mol. Pharmaceutics* **2009**, *6*, 1388.
(19) Jain, P.; Pradeep, T. *Biotechnol. Bioeng.* **2005**, *90*, 59.
(20) Sharma, V. K.; Yngard, R. A.; Lin, Y. *Adv. Colloid Interface Sci.* **2009**, *145*, 83.
(21) Gopinath, P.; Gogoi, S. K.; Chattopadhyay, A.; Ghosh, S. S. *Nanotechnology* **2008**, *19*, 75104.
(22) Gopinath, P.; Gogoi, S. K.; Sanpui, P.; Paul, A.; Chattopadhyay, A.; Ghosh, S. S. *Colloids Surf., B* **2010**, *77*, 240.
(23) Hsin, Y.-H.; Chen, C.-F.; Huang, S.; Shih, T.-S.; Lai, P.-S.; Chueh, P. J. *Toxicol. Lett.* **2008**, *179*, 130.
(24) Newmeyer, D. D.; Ferguson-Miller, S. *Cell* **2003**, *112*, 481.
(25) Thompson, C. B. *Science* **1995**, *267*, 1456.
(26) AshaRani, P. V.; Mun, G. L. K.; Hande, M. P.; Valiyaveettil, S. *ACS Nano* **2009**, *3*, 279.
(27) Asharani, P. V.; Wu, Y. L.; Gong, Z.; Valiyaveettil, S. *Nanotechnology* **2008**, *19*, 255102.
(28) Ott, M.; Gogvadze, V.; Orrenius, S.; Zhivotovsky, B. *Apoptosis* **2007**, *12*, 913.
(29) Carr, C.; Ng, J.; Wigmore, T. *Curr. Anaesth. Crit. Care* **2008** *19*, 70.
(30) Singal, P. K.; Iliskovic, N. *New Engl. J. Med.* **1998**, *339*, 900.
(31) Peer, D.; Karp, J. M.; Hong, S.; Farokhzad, O. C.; Margalit, R.; Langer, R. *Nat. Nanotechnol.* **2007**, *2*, 751.
(32) Lu, Z.; Yeh, T.; Tsai, M.; Au, J. L.; Wientjes, M. G. *Clin. Cancer Res.* **2004**, *10*, 7677.
(33) Dreis, S.; Rothweiler, F.; Michaelis, M.; Cinatl, J.; Kreuter, J.; Langer, K. *Int. J. Pharm.* **2007**, *341*, 207.
(34) Sahu, A.; Kasoju, N.; Bora, U. *Biomacromolecules* **2008**, *9*, 2905.
(35) Kumar, M. N. V. R.; Muzzarelli, R. A. A.; Muzzarelli, C.; Sashiwa, H.; Domb, A. J. *Chem. Rev.* **2004**, *104*, 6017.
(36) Bhattarai, N.; Gunn, J.; Zhang, M. *Adv. Drug Delivery Rev.* **2010**, *62*, 83.
(37) Murugadoss, A.; Chattopadhyay, A. A *Nanotechnology* **2008**, *19*, 015603.
(38) Calvo, P.; Remunan-Lopez, C.; Vila-Jato, J. L.; Alonso, M. J. *J. Appl. Polym. Sci.* **1997**, *63*, 125.
(39) Weston, S. A.; Parish, C. R. *J. Immunol. Methods* **1990**, *133*, 87.
(40) Lee, D. W.; Yun, K. -S.; Ban, H. -S.; Choe, W.; Lee, S. K.; Lee, K. Y. *J. Controlled Release* **2009**, *139*, 152.
(41) Arora, S.; Jain, J.; Rajwade, J. M.; Paknikar, K. M. *Toxicol. Lett.* **2008**, *179*, 93.
(42) Hussain, S. M.; Hess, K. L.; Gearhart, J. M.; Geiss, K. T.; Schlager, J. J. *Toxicol. in Vitro* **2005**, *19*, 975.
(43) Rello, S.; Stockert, J. C.; Moreno, V.; G'amez, A.; Pacheco, M.; Juarranz, A.; Cãnete, M.; Villanueva, A. *Apoptosis* **2005**, *10*, 201.
(44) Allen, R. T.; Hunter, W. J., III; Agrawal, D. K. *J. Pharmacol. Toxicol. Methods* **1997**, *37*, 215.
(45) Martin, S. J.; Reutelingsperger, C. P. M.; McGahon, A. J.; Radar, A.; van-Schie, R. C.; LaFace, D. M.; Green, D. R. *J. Exp. Med.* **1995**, *182*, 1545.
(46) Koopman, G.; Reutelingsperger, C. P.; Kuijten, G. A.; Keehnen, R. M.; Pals, S. T.; van Oers, M. H. *Blood* **1994**, *84*, 532.
(47) Nunez, G.; Benedict, M. A.; Hu, Y.; Inohara, N. *Oncogene* **1998**, *17*, 3237.
(48) Janicke, R. U.; Sprengart, M. L.; Wati, M. R.; Porter, A. G. *J. Biol. Chem.* **1998**, *273*, 9357.
(49) Thress, K.; Kornbluth, S.; Smith, J. J. *J. Bioenergetics Biomembranes* **1999**, *31*, 321.
(50) Cossarizza, A.; Baccarani-Contri, M.; Kalashnikova, G.; Franceschi, C. *Biochem. Biophys. Res. Commun.* **1993**, *197*, 40.
(51) Foley, S.; Crowley, C.; Smaihi, M.; Bonfils, C.; Erlanger, B. F.; Seta, P.; Larroque, C. *Biochem. Biophys. Res. Commun.* **2002**, *294*, 116.
(52) Limbach, L. K.; Wick, P.; Manser, P.; Grass, R. N.; Bruinink, A.; Stark, W. J. *Environ. Sci. Technol.* **2007**, *41*, 4158.
(53) Sayes, C. M.; Gobin, A. M.; Ausman, K. D.; Mendez, J.; West, J. L.; Colvin, V. L. *Biomaterials* **2005**, *26*, 7587.
(54) Green, M.; Howman, E. *Chem. Commun.* **2005**, *121*, 121.
(55) Park, E. J.; Choi, J.; Park, Y.; Park, K. *Toxicology* **2008**, *245*, 90.
(56) Quillet-Mary, A.; Jaffre'zou, J. −P.; Mansat, V.; Bordier, C.; Naval, J.; Laurent, G. *J. Biol. Chem.* **1997**, *272*, 21388.
(57) Wataha, J.; Lockwood, P.; Schedle, A. *J. Biomed. Mater. Res.* **2000**, *52*, 360.
(58) Thubagere, A.; Reinhard, B. M. *ACS Nano* **2010**, *4*, 3611.
(59) Gil, P. R.; Oberdorster, G.; Elder, A.; Puntes, V.; Parak, W. J. *ACS Nano* **2010**, *4*, 5527.
(60) Freeman, S. M.; Abboud, C. N.; Whartenby, K. A.; Packman, C. H.; Koeplin, D. S.; Moolten, F. L.; Abraham, G. N. *Cancer Res.* **1993**, *53*, 5274.
(61) Gopinath, P.; Ghosh, S. S. *Mol. Cell. Biochem.* **2009**, *324*, 21.
(62) Yang, S.-J.; Lin, F.-H.; Tsai, K.-C.; Wei, M.-F.; Tsai, H.-M.; Wong, J.-M.; Shieh, M.-J. *Bioconjugate Chem.* **2010**, *21*, 679.